Fluorinated Zinc Phthalocyanine as Donor for Efficient Vacuum-Deposited Organic Solar Cells

*Jan Meiss, Andre Merten, Moritz Hein, Christoph Schuenemann, Stefan Schäfer, Max Tietze, Christian Uhrich, Martin Pfeiffer, Karl Leo, and Moritz Riede**

Efficient single bulk heterojunction organic solar cells based on blends of a fluorinated zinc phthalocyanine as electron donor and fullerene C_{60} as electron acceptor are reported. In comparison to the commonly used absorber zinc phthalocyanine, the fluorination of the molecule to F_4ZnPc leads to an increase in ionisation potential and subsequently to an improvement of about 170 mV in the open circuit voltage of organic solar cells, while the short circuit current density and fill factor remain nearly unchanged. Similar to ZnPc:C_{60}-based devices, the device characteristics of F_4ZnPc:C_{60} solar cells can be further enhanced by improving the blend layer morphology by substrate heating during deposition. F_4ZnPc is an efficient donor material that can achieve a 4.6% power conversion efficiency in single heterojunction organic solar cells.

1. Introduction

In recent years, organic solar cells (OSCs) have emerged as promising solar cell technology: the potential to fabricate flexible, lightweight devices with low material consumption and tunable absorption characteristics opens a pathway to cost-efficient electricity generation. A better understanding of this field offers challenges for chemists, physicists, material scientists, and theoreticians alike, providing opportunities for joint studies. Increasing research efforts have steadily improved power conversion efficiencies (η) since the first efficient bilayer photovoltaic device was reported by Tang.[1] For vacuum deposited, small molecule-based OSCs, the highest reported efficiencies for single heterojunction devices so far are about 5% with oligothiophene donors.[2,3] Tandem OSCs with naphthalocyanine/phthalocyanine combinations have reached 5.2%,[4] phthalocyanine/oligothiophene devices have been shown to achieve 6.07%,[5] and could also be modified in such a way that semitransparent devices with 4.9% efficiency and transparency in the visible range were combined.[6] With proprietary materials, certified power conversion efficiencies of 8.3% have been achieved.[7] The latter is on par with efficiencies that have recently been shown for single heterojunction solution-processed polymer-based OSCs.[7]

To make OSCs commercially viable, much research is focused on further improving the efficiency. Central to these efforts are donor and acceptor absorber materials, which serve for light absorption, exciton generation and transport, provide the interface for exciton separation, and have to efficiently transport the charges to the respective contacts. This requires adjusting the energy levels for better absorption of the solar spectrum, for reducing energy losses, and improving morphology and transport properties. The material class of phthalocyanines has been extensively used as electron donor in the field of small-molecule OSCs.[8] The usual structural variations are only on the central metal atom, but there are other options for modifications, e.g., halogenation. Perfluorinated phthalocyanines have been investigated by several groups as alternative acceptor molecule[9,10] or in recombination contacts,[11] and zinc phthalocyanine (ZnPc) derivatives with phenyl or larger substituents have been considered recently.[12] In combination with C_{60} as the electron acceptor, unsubstituted ZnPc exhibits good transport properties and absorption, high short circuit current densities j_{sc} and fill factors FF, but is limited by a low open circuit voltage V_{oc}. The optical gap of ZnPc is about 1.6 eV. However, the difference between ionisation potential (IP) of ZnPc and electron affinity (EA) of C_{60} is about 1.1 eV,[13–16] and typical V_{oc} is only around 0.5 ± 0.05 V.[17–22] Thus, at least 65% of the energy of each photon is lost during energy conversion. Hence, much research is devoted to shifting energy levels to change the absorption spectrum and/or to increase V_{oc}, while at the same time retaining high charge separation efficiency and transport properties.[23–25]

In this paper, we present a fluorinated version of zinc phthalocyanine, which shows nearly identical absorption and transport properties as ZnPc. OSC devices demonstrate that, even with thick blend layers, high efficiencies of over 4% are achieved. The devices greatly profit from substrate heating, which is demonstrated in further experiments. Optimized heated F_4ZnPc-based OSC are compared in performance to non-modified ZnPc. We show that V_{oc} is significantly improved by 30%, with a

Dr. J. Meiss, Dr. A. Merten, M. Hein, C. Schuenemann, M. Tietze, Prof. K. Leo, Dr. M. Riede
Institut für Angewandte Photophysik
Technische Universität Dresden
George-Bähr-Str. 1, 01069 Dresden, Germany
E-mail: moritz.riede@iapp.de
Dr. S. Schäfer
Robert Bosch GmbH, Robert-Bosch-Platz 1, 70839 Gerlingen, Germany
Dr. C. Uhrich, Dr. M. Pfeiffer
Heliatek GmbH, Treidlerstr. 3, 01139 Dresden, Germany

DOI: 10.1002/adfm.201101799

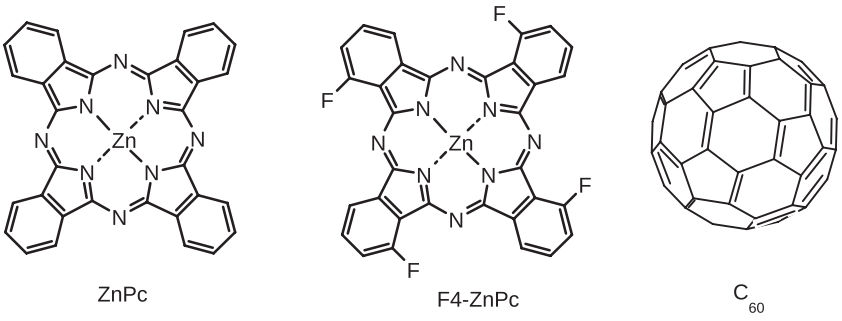

Figure 1. Chemical structure of the electron donor molecules zinc phthalocyanine (ZnPc), fluorinated zinc phthalocyanine (F_4ZnPc), and the electron acceptor molecule C_{60} used in the photovoltaic active layers.

corresponding increase of η by 30%, if ZnPc is replaced by F_4ZnPc in an otherwise identical stack in terms of j_{sc} and FF.

2. Results and Discussion

2.1. Materials

Molecular energy levels can be modified by, e.g., substitution of hydrogen ligands by more or less electronegative species, such as fluorine or CH_3, respectively. This does not necessarily influence the HOMO-LUMO (highest occupied molecular orbital–lowest unoccupied molecular orbital) gap, as shown by Mayer et al.[26] Fluorine is known to be a strong acceptor and can be used to lower molecular energy levels. One example is tetracyanoquinodimethane (TCNQ) that can be used as p-dopant as tetrafluoro-TCNQ (F4-TCNQ).[27] Even C_{60} can be turned into an efficient p-dopant with sufficient fluorination.[28] Another example is the addition of 16 fluorine atoms to ZnPc or CuPc, which lowers the IP of the resulting perfluorinated derivatives by over 1.5 eV with respect to the unmodified molecule and leads to an n-type material.[10,29] Thus, perfluorination is too strong for use with ZnPc as electron donor and fewer F atoms are required for the engineering of suitable energy levels. **Figure 1** displays the chemical structure of a ZnPc containing only four F atoms, along with the structures of unsubstituted ZnPc and C_{60}. The synthesis route is described elsewhere.[30]

Figure 2 shows ultraviolet photoelectron spectroscopy (UPS) measurements of the high binding energy cutoff (HBEC) and the hole injection barrier (HIB) of 15 nm ZnPc and 12 nm F_4ZnPc on Au. The UV lamp provides photons with an energy $h\nu = 21.22$ eV. The IP is then calculated as,

$$\mathrm{IP} = h\nu - (E_{\mathrm{HBEC}} - E_{\mathrm{HIB}}). \quad (1)$$

We measure a HBEC of 16.79 eV and a HIB of 1.03 eV for F_4ZnPc, leading to IP = 5.46 eV. For the unsubstituted ZnPc, an IP of 5.07 eV is determined (HBEC = 17.32 eV; HIB = 1.17 eV), similar to values reported in the literature.[13,14,31] Semi-empirical calculations of the energy levels of F_4ZnPc in the gas phase[32] yielded a HOMO of F_4ZnPc which is is 0.22 eV deeper compared to ZnPc, confirming our experimental results.[26] For the electron acceptor C_{60}, the electron affinity (EA) is reported to be about 4 eV.[15,16,33] Defining the effective bandgap as

$$E_{\mathrm{g,eff}} = \mathrm{IP}_{\mathrm{donor}} - \mathrm{EA}_{\mathrm{acceptor}} \quad (2)$$

we find $E_{\mathrm{g,eff}}$ of 1.46 eV for F_4ZnPc and 1.07 eV for ZnPc, respectively, based on our UPS measurements. Several studies document a linear proportionality of V_{oc} and $E_{\mathrm{g,eff}}$,[34,35] thus we expect that V_{oc} for OSC with F_4ZnPc as donor should exhibit V_{oc} that are 0.22–0.39 eV higher than identical ZnPc-based devices.

Whereas the fluorination of the ZnPc has a significant effect on its IP, the changes in extinction coefficient, as shown in **Figure 3**, are small. The F_4ZnPc:C_{60} is deposited with the substrate being heated to 104 °C, but substrate heating does not cause a qualitative difference of the optical properties (data not shown). Thus, the optical gap of F_4ZnPc appears rather unchanged.

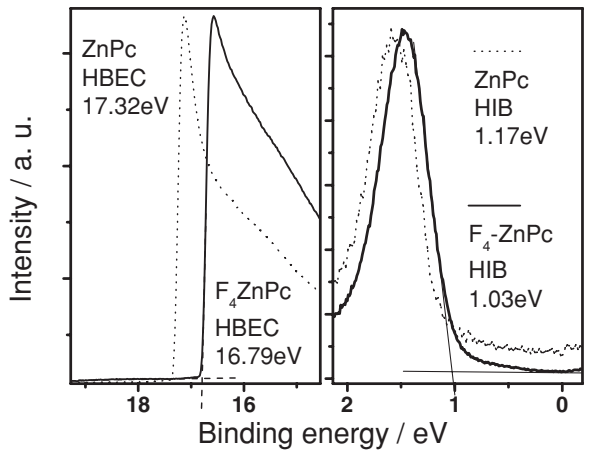

Figure 2. UPS measurements of the HBEC and HIB of 12 nm F_4ZnPc on Au (solid lines). For comparison, the corresponding curves of 15 nm ZnPc on Au are shown as dotted black lines.

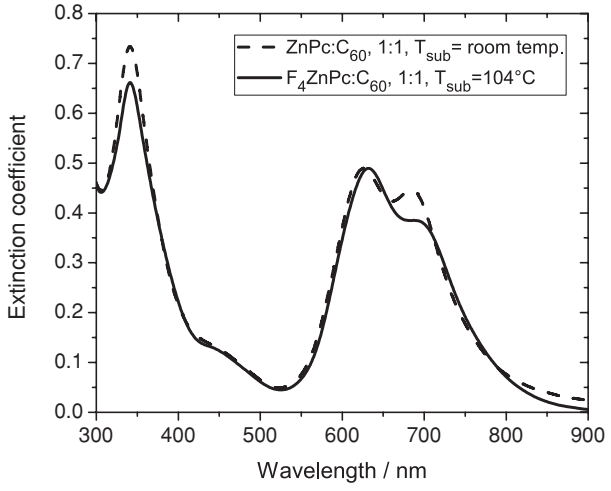

Figure 3. Extinction coefficient of ZnPc:C_{60} (1:1) and F_4ZnPc:C_{60} (1:1) as determined from reflection and transmission measurements.

Both ZnPc and F_4ZnPc exhibit strong absorption in a broad part of the solar spectrum, with the main peak in the orange-red starting at about 550 nm and extending to the dark red up to 800 nm. The extinction coefficient of ZnPc has main peaks in the red at 626 and 684 nm, with absorption coefficients of 98 400 and 82 000 cm^{-1}, respectively; F_4ZnPc also shows the first peak slightly red-shifted at 632 nm (98 200 cm^{-1}), but only exhibits a shoulder at 684 nm. The redshift of the first peak hints at higher structural order with stronger charge carrier delocalization. The transformation of the second peak of ZnPc to a shoulder of F_4ZnPc is attributed to modified intermolecular interactions, which are caused by the F atoms.[36] Previous studies found spectra typical for the α phase; differences of ZnPc and F_4ZnPc were attributed to different coupling of transition dipoles.[9] We have measured the hole mobility of F_4ZnPc:C_{60} and ZnPc:C_{60} in BHJ with a 1:1 mixing ratio by volume on organic field effect transistors (OFET). Preliminary results show that the values are in the same order of magnitude with 1.4×10^{-5} and 8.3×10^{-5} cm^2 V^{-1} s^{-1}, respectively. The lower mobility of F_4ZnPc:C_{60} may be attributed to a lower overlap of the π-electron system due to higher intermolecular distances.

2.2. OSC with F_4ZnPc:C_{60} Bulk Heterojunctions

A series of devices with F_4ZnPc as donor and C_{60} as acceptor in bulk heterojunctions (BHJ) is prepared. The BHJ thickness t_b is varied in a wide range from 25–85 nm to evaluate the transport properties of the bulk, the influences on FF and j_{sc}, and to find the optimum device performance. All investigated devices are based on the p-i-n concept and prepared by vacuum deposition.[37,38] The corresponding stacks are illustrated in **Figure 4**. Indium tin oxide (ITO) serves as transparent electrode, but the layer structures are inverted: depositing 5 nm C_{60} doped with NDN1 directly onto the ITO leads to an ohmic contact and allows for an efficient collection of electrons. The photovoltaic active layer is a combination of 10 nm pristine C_{60} and a BHJ consisting of F_4ZnPc:C_{60} in a 1:1 mixing ratio (by volume). The BHJ has different thicknesses t_b between 25–85 nm. For the hole transport layer (HTL), *N,N′*-diphenyl-*N,N′*-bis{4′-[*N,N*-bis(naphth-1-yl)-amino]-biphenyl-4-yl}-benzidine (Di-NPB; IP = 5.33 eV) doped with NDP9 is used, followed by a 1 nm NDP9 layer and a reflective Al back contact for hole collection. All layers are deposited with the substrate held at room temperature (RT). The stacks are based on basic optical simulations, and the HTL thickness t_{HTL} is varied between 30–50 nm such that the absorbing BHJ is in the optimum position of the optical field distribution of the OSC.

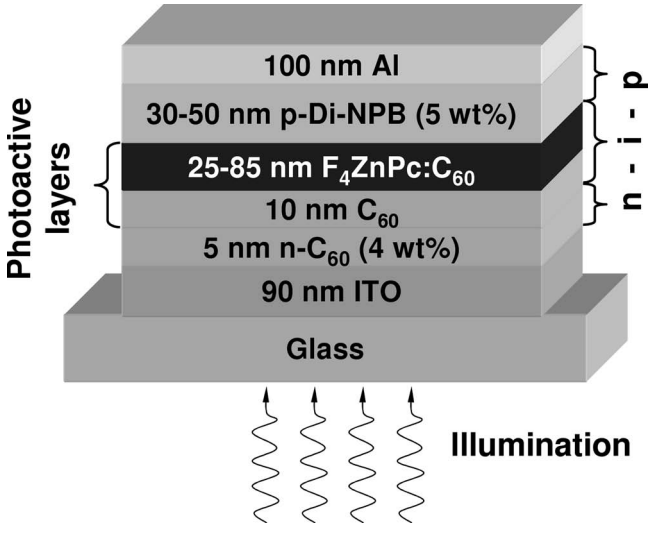

Figure 4. Solar cell device stack for the F_4ZnPc:C_{60} devices that are prepared on substrates at RT. Depending on the thickness of the F_4ZnPc:C_{60} layer, the thickness of the p-doped Di-NPB layer is varied for optical optimization.

Table 1. Summary of the current–voltage parameters, averaged for four F_4ZnPc:C_{60} devices for each thickness t_b of the bulk layer. The value of t_{HTL} represents the HTL layer thickness. All efficiencies are corrected for spectral mismatch. The F_4ZnPc devices were measured under (95 ± 1) mW cm^{-2} illumination.

t_b [nm]	V_{oc} [V]	j_{sc} [mA cm^{-2}]	*FF* [%]	η [%]	t_{HTL} [nm]
25	0.73	6.6 ± 0.1	60	3.1 ± 0.1	50
45	0.73	9.2 ± 0.1	50	3.5 ± 0.1	40
55	0.73	10.1 ± 0.2	47	3.6 ± 0.1	40
65	0.73	10.6 ± 0.2	45	3.6 ± 0.1	35
75	0.73	10.8 ± 0.2	43	3.5 ± 0.1	30
85	0.73	10.7 ± 0.2	40	3.3 ± 0.1	30

The measurement results and corresponding layer thicknesses are summarized in **Table 1**. Current–voltage curves in the dark and under illumination are depicted in **Figure 5**.

The *j*(*V*) curves of the OSC in the dark (Figure 5a) illustrate that the highest parallel resistances, lowest series resistances, and highest currents are observed for thin blend layers (e.g., 25 nm). The series resistance then increases with increasing blend thickness up to 85 nm. Under reverse bias, the dependency of current density at –1.0 V on blend layer thickness is even more pronounced: the highest absolute current density of $j \approx 4 \times 10^{-2}$ mA cm^{-2} is found for 25 nm F_4ZnPc:C_{60}; this is lower by one order of magnitude for 85 nm F_4ZnPc:C_{60}. We conclude from this that the main influence on parallel resistance stems from the bulk heterojunction and not from electrode contacts or charge carrier transport layers; possible reasons may be dead-ends or isolated donor or acceptor grains in the BHJ, which become more likely for thicker blends. Another factor may be the lower t_{HTL} for high t_b (e.g., 30 nm p-Di-NPB for 85 nm F_4ZnPc, compared to 50 nm p-Di-NPB for 25 nm F_4ZnPc): the HTL acts as buffer layer to avoid direct contact between blend and top electrode. If the blend layer is very thick, this may result in a rough surface that cannot completely be covered by a thin HTL.

Under illumination, $V_{oc} \approx 0.5 \pm 0.05$ V is usually obtained for OSC with a blend of ZnPc and C_{60}.[17–22] The corresponding OSCs with F_4ZnPc show higher voltages of 0.73 V, originating from the difference in IP of the fluorinated material which is approximately 0.22–0.39 eV higher compared to non-fluorinated ZnPc. V_{oc} is independent of t_b and hence of j_{sc}. This indicates

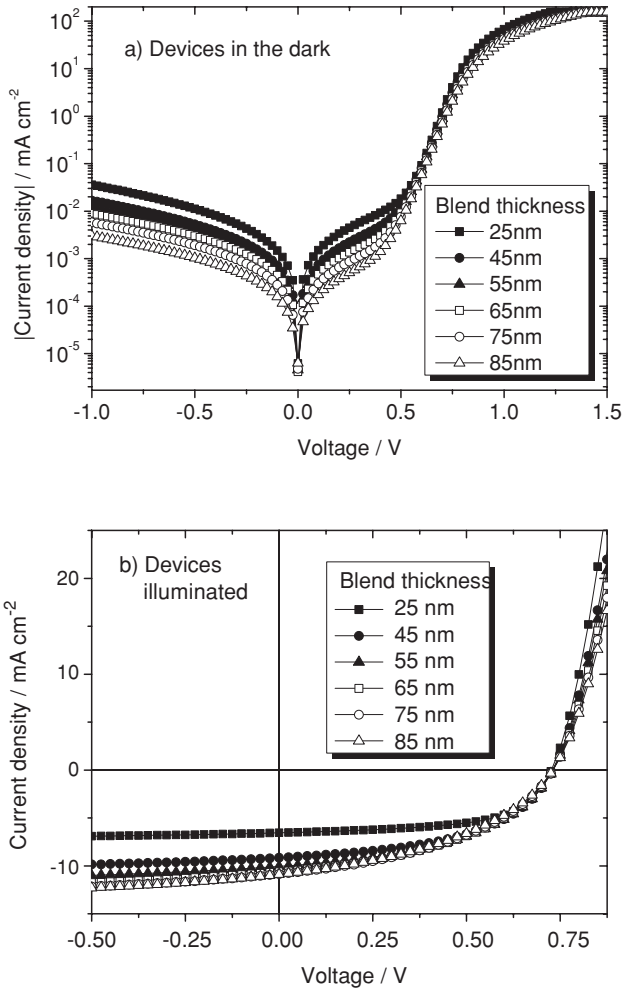

Figure 5. Current–voltage characteristics of solar cells where F_4ZnPc:C_{60} of different thicknesses is deposited on an unheated substrate. The top graph (a) shows a log–lin plot of the dark $j(V)$ curves and the bottom graph (b) the same devices under illumination. The blend thickness t_b is varied with t_b = 25 nm (squares), 45 nm (circles), 55 nm (triangles), 65 nm (empty squares), 75 nm (empty circles), or 85 nm (empty triangles).

that the quasi-Fermi level splitting is not decisively influenced by the differences in j_{sc}, but that the energy level alignment is the dominating factor.

The high FF of 60% for t_b = 25 nm is similar to the highest reported vlues for ZnPc in the literature, but drops to 40% for 85 nm thick blend layers. **Figure 6** illustrates the dependence of FF on t_b and documents how the FF decreases for higher BHJ blend thicknesses t_b. In forward bias, the electrical field in the donor:acceptor blend has a smaller intensity for increasing t_b, which is disadvantageous for charge carrier collection efficiency and hence increases recombination. Furthermore, high t_b increases the probability of isolated clusters of donor or acceptor material that are not connected to transport layers or electrodes. Such dead-ends increase charge carrier recombination, which reduces FF. Also, for thick BHJ, separated charge carriers have to travel a longer distance from the location of dissociation to the dedicated HTL or ETL. Imbalanced mobilities of donor and acceptor can hence be expected to become more important for higher t_b and may negatively influence device performance.

Such explanations are supported by the fact that j_{sc} peaks at t_b = 75 nm, as is evident from Figure 6, and then slightly drops at t_b = 85 nm. If the BHJ thickness is further increased, even more photons are absorbed. However, internal losses mount and decrease the number of charge carriers that can successfully be extracted.

The dependence of peak EQE (at 635 nm) on t_b is illustrated in the right part of Figure 6. We see that EQE increases for devices with 25–65 nm with BHJ thickness, but then saturates at t_b > 65 nm. A similar trend is seen in the overall EQE in **Figure 7** (albeit less pronounced, due to the dependence of EQE on the optical field distribution): a clear increase in a broad spectral range is seen up to t_b = 55 nm, but this saturates at 60–65% in the red range (600–750 nm).

The EQE data document that under monochromatic illumination (relatively low charge carrier density), excellent photon harvesting is possible. However, the saturation of j_{sc} and EQE with high t_b is concomitant with a drop in FF due to limitations in charge carrier extraction. This leads to a maximum η and an optimal t_b of 55–65 nm, as seen in Figure 6.

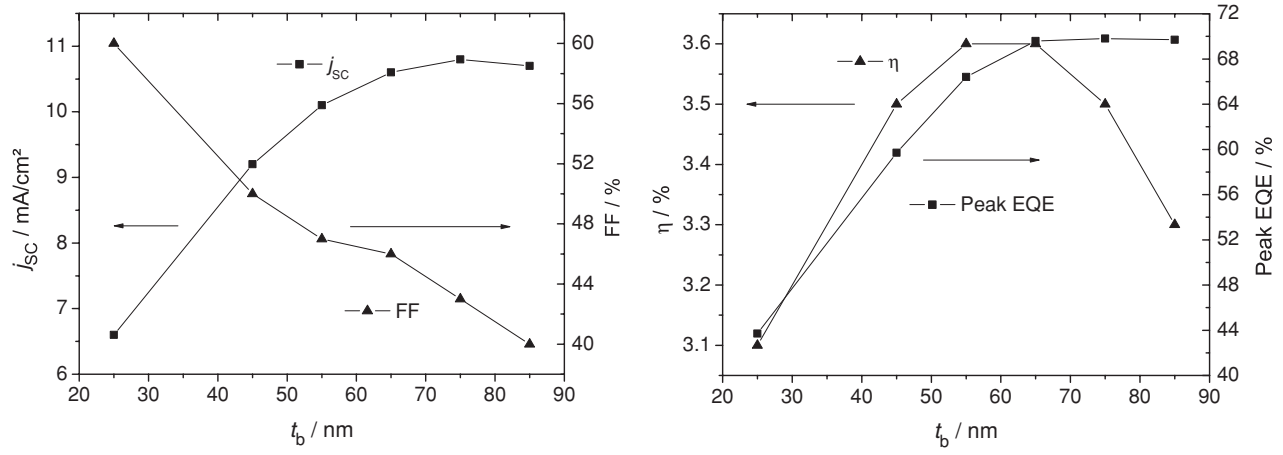

Figure 6. Dependence of OSC parameters j_{sc}, η, FF, and peak EQE on t_b, with t_b ranging from 25–85 nm.

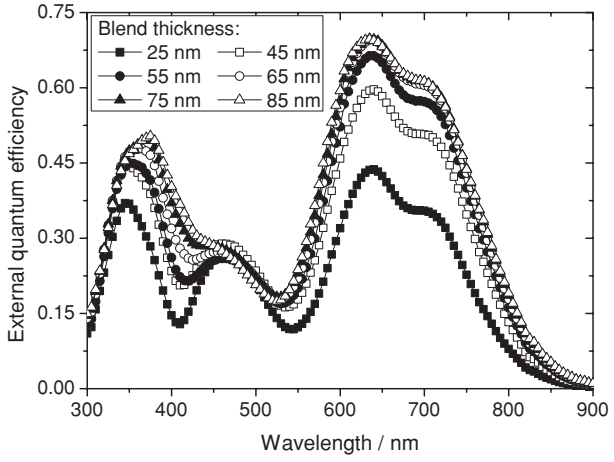

Figure 7. External quantum efficiency of $F_4ZnPc:C_{60}$-containing OSC, deposited with the substrate at RT, with blend thicknesses ranging from 25–85 nm.

In summary, despite a strong reduction in FF at very high BHJ thicknesses, all OSCs reach high photocurrents and acceptable FF even at high t_b, which leads to $\eta > 3\%$ for all devices and all t_b. The best performance is achieved at $t_b = 55$–65 nm with $\eta = 3.6\%$. This is beyond the efficiencies of of ZnPc-based OSCs, as they usually are reported with $\eta < 3\%$ in the literature, mostly due to a lower V_{oc}. Hence, we conclude that F_4ZnPc is an excellent candidate to replace the commonly used CuPc or ZnPc.

2.3. Morphology

Previous studies showed that heating of the substrate during film deposition can have a significant impact on layer morphology and performance of $ZnPc:C_{60}$-based solar cells.[39–41] Given the similar structure of F_4ZnPc and ZnPc, we study the influence of substrate heating on morphology of $F_4ZnPc:C_{60}$ during BHJ deposition to investigate if similar effects are observed. We evaporate layers consisting of 150 nm blend onto glass pre-coated with 20 nm C_{60}, with the substrate either heated to $t_{sub} = 110$ °C, or unheated during BHJ dposition. The fullerene sublayer is chosen to simulate realistic conditions for the absorber layer, because the solar cells consist of a nip-structure with C_{60} as sublayer below the BHJ (see Figure 4). The resulting AFM micrographs are depicted in **Figure 8**. The top row shows measurements of a sample where the mixed layer is deposited onto an unheated substrate; the sample in the bottom row is evaporated onto a substrate heated to 110 °C, which had been found as optimal t_{sub} for processing of solar cell samples in previous studies.[40]

The images of unheated layers do not show clear structures and are relatively smooth with a root mean square roughness $R_{rms} = 0.7$ nm. Substrate heating increases R_{rms} to 2.7 nm and leads to visible grains. We attribute this to a partial phase separation of donor and acceptor, as has also been observed for ZnPc in the past.[39,40,42]

The AFM images are compared to scanning electron microscopy (SEM), with the results shown in **Figure 9**. Both methods lead to the same conclusion: heating of the substrate during deposition of the $F_4ZnPc:C_{60}$ BHJ dramatically changes surface layer morphology and roughness, towards more grainy features, as already observed for $ZnPc:C_{60}$ blends.[41]

To investigate the potential presence of crystallinity in more detail, X-ray diffraction measurements (XRD) are carried out. Using XRD with Cu K_α radiation, a single peak at around 6.8° is found for 36 nm thick ZnPc films grown on ITO (see **Figure 10**a). This peak is attributed to the α-ZnPc with (010)-orientation.[43,44] In this triclinic crystal structure ZnPc stacks in parallel columns.[43,44] For ITO, peaks are observed at $2\theta = 21°$ and 30° which are attributed to the (211) and (222) orientation of the ITO body-centered cubic (bcc) crystal structure.[45]

Like ZnPc, intrinsic F_4ZnPc forms a polycrystalline thin film with a single peak visible at 6.6° in XRD (see Figure 10a). The slightly shifted peak position is an indication of a different spacing of the molecules in the crystal or a change in the crystal structure. Effects of bulky side groups of phthalocyanines on the crystal structure have already been reported by Bruder et al.[12] For relatively small phenyl side groups, the same stacking was observed and only the intermolecular distance was changed.[12] This corresponds to studies of intrinsic ZnPc where crystallites are found by XRD[42] and wide-angle XRD.[41]

For 70 nm $F_4ZnPc:C_{60}$ blends (1:1 ratio), there are no peaks visible in the XRD diffractograms (see Figure 10b) that could

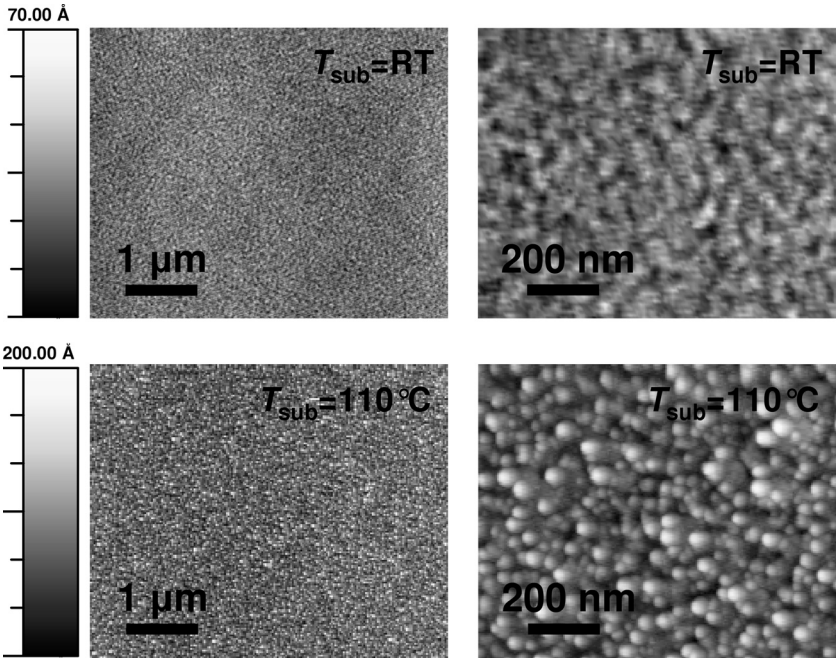

Figure 8. AFM micrographs of $F_4ZnPc:C_{60}$ (1:1 volume ratio), deposited on unheated (top) and heated (bottom) substrates. Two different scan sizes are used for each substrate temperature to better illustrate the effect of heating: 5×4 µm^2 (left), and 1×0.8 µm^2 (right). The scale bar of the unheated samples (7 nm) is much smaller compared to the 20 nm of the heated samples since the roughness increases significantly if the blend is deposited on a heated substrate.

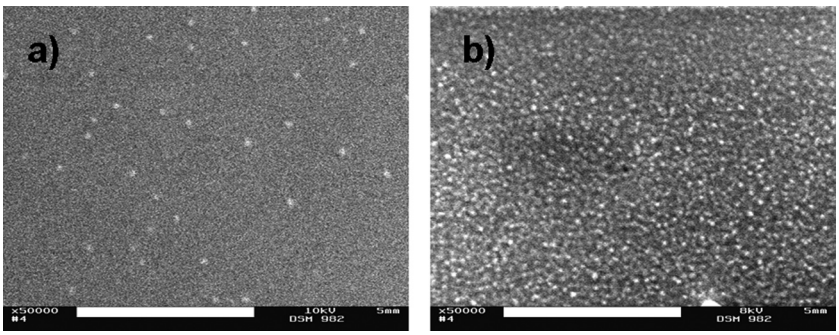

Figure 9. SEM micrographs of $F_4ZnPc:C_{60}$ (1:1 volume ratio), deposited on unheated (a) and heated to 104 °C (b) substrates. The white scale bars represent 1 µm.

be associated with organic materials. This indicates that these films are at least X-ray amorphous, which was also observed by Maennig et al.[46,47] using electron diffraction for $ZnPc:C_{60}$ blends that were deposited at room temperature. X-ray studies of similar $F_4ZnPc:C_{60}$ samples where the substrate was kept at 110 °C during deposition revealed that, even then, the blend layers are X-ray amorphous and no crystal structure could be obtained (data not shown).

A systematic study of $ZnPc:C_{60}$ BHJ-based OSC with substrate temperature variations from RT to 80, 90, 100, 110, 120, and 130 °C revealed that an optimum device performance is reached at 110 °C, mediated by an optimum in FF and

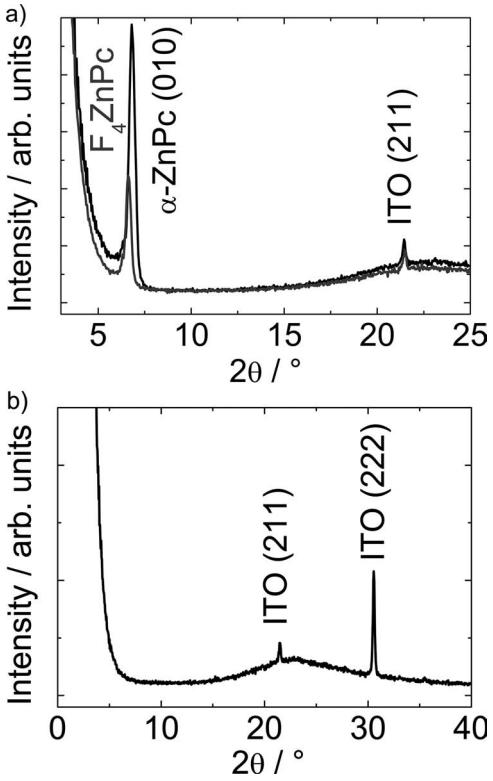

Figure 10. XRD spectra of 36 nm thick ZnPc and F_4ZnPc films (a) and 70 nm thick $F_4ZnPc:C_{60}$ blends grown on ITO (b). In the neat films the peaks at 6.6° and 6.8° are attributed to F_4ZnPc and ZnPc, respectively; in the blend layer, only ITO peaks are observed.

j_{sc}.[40] A phase separation, with a possible formation of an interpenetrating network in the blend, was given as tentative explanation. We expect comparable behaviour from $F_4ZnPc:C_{60}$ due to the similar molecular structures. However, despite extensive studies, there is no completely clear picture regarding the structure formation of ZnPc-containing films. On the one hand, intrinsic ZnPc and F_4ZnPc layers exhibit crystalline features, as shown in this work and elsewhere.[41,42,46] Substrate heating may in fact be a rather minor factor regarding the presence of crystallites both for ZnPc[42] and F_4ZnPc (present study, data not shown). In contrast to that, studies of BHJ are inconclusive. Suemori and co-workers report on highly crystalline metal-free phthalocyanine at 80 °C substrate temperature, but did not present the corresponding XRD data.[39] Pfuetzner and co-workers found no indication for crystallites in BHJ by wide angle XRD, independent of the substrate temperature.[41] Transmission electron micrographs (TEM) of BHJ on Cu grids at room temperature exhibited amorphous features, and this was confirmed by absorption measurements.[41,46] The only potential hint at possible changes in layer structure were TEM of BHJ on Cu grid at 110 °C that were attributed to monoclinic ZnPc;[41] however, since the substrate is often a decisive parameter for layer growth, we consider this a rather special case.

Due to overwhelming evidence, we assume that we do not have major F_4ZnPc crystallization in the BHJ of our devices, independent of the substrate temperature. All samples here and in the literature were X-ray amorphous. However, we have found qualitative morphological changes by AFM and SEM. To follow up on this, we choose $T_{sub} \approx 105$ °C that has proven to be optimal for $ZnPc:C_{60}$ in the literature[40] and test this parameter in OSC.

2.4. OSC with $F_4ZnPc:C_{60}$ Deposited on Heated Substrates

Our microscopical investigations confirm a significant impact of substrate heating on morphology of $F_4ZnPc:C_{60}$ blend layers, as was already observed for $ZnPc:C_{60}$ layers.[40,42] In addition, the hole and electron mobilities of ZnPc and C_{60}, respectively, were found to be positively influenced by heating.[41] Thus, we investigate whether solar cells using $F_4ZnPc:C_{60}$ BHJ reflect such findings, and if crucial device parameters can be as positively influenced as for $ZnPc:C_{60}$ BHJ. A variation of blend layer thickness t_b is ideal for this purpose since the heating effect is especially pronounced for thick blends.[40]

The layer stack is shown in **Figure 11** and is similar to the one used for the unheated devices (see Figure 4). We compare samples with t_b between 45 and 65 nm for which the substrate is kept at $t_{sub} = 104$ °C during deposition of the mixed layer. To exclude optical effects obscuring the influence of heating, the hole transport layer thickness t_{HTL} between absorber and reflective metal back contact is kept constant with a thickness of 30 nm. As reference, an optimized device with ZnPc as donor is created in parallel for a direct comparison to devices with F_4ZnPc as donor.

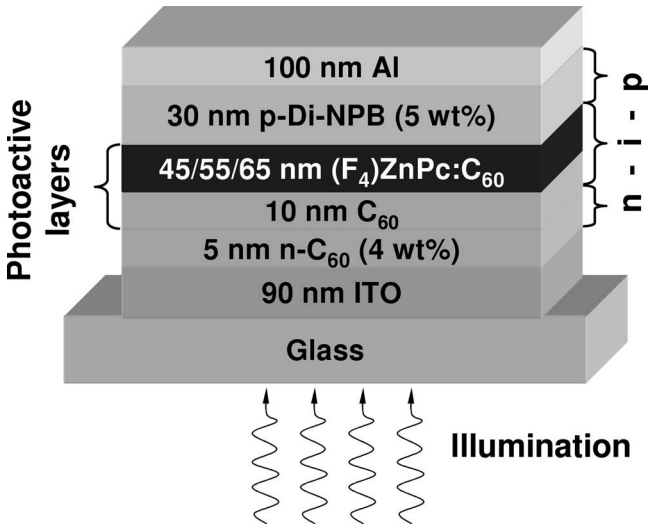

Figure 11. Solar cell device stack for the ZnPc:C_{60} and F_4ZnPc:C_{60} devices, t_{sub} = 104 °C.

Figure 11 shows the stack structures for solar cells with either ZnPc or F_4ZnPc as donor materials and C_{60} as acceptor. The corresponding $j(V)$ curves in the dark and under simulated sun light are shown in **Figure 12** and summarized in **Table 2**. EQE is presented in **Figure 13**.

The dark $j(V)$ curves of all devices are shown in Figure 12a. All three solar cells with F_4ZnPc exhibit very similar behaviour in forward bias, suggesting that the differences in t_b do not strongly influence the series resistance. The current density in forward direction is higher for the ZnPc-containing device by more than an order of magnitude for $V > 0.2$ V. We attribute this to higher bulk recombination due to the smaller effective bandgap for OSC containing ZnPc:C_{60} instead of F_4ZnPc:C_{60}. Both BHJ-based OSC are clearly limited by bulk recombination because the doped transport layers effectively suppress recombination at the electrodes.[48]

The reference ZnPc:C_{60} device exhibits a typical V_{oc} = 0.52 V. Due to the higher IP of F_4ZnPc, solar cells using F_4ZnPc can achieve about 0.16 V higher V_{oc} than devices using ZnPc. However, this is slightly less than the measured 0.2–0.4 eV difference in IP which might indicate differences in ground state interaction with C_{60}; such differences may influence V_{oc} via the formation of dipoles or by changing the recombination dynamics at applied voltages close to V_{oc}. The voltage of F_4ZnPc-containing devices is higher by approximately 30%, which boosts the power conversion efficiency accordingly.

The data demonstrate that generally, higher blend layer thicknesses t_b of F_4ZnPc:C_{60} generate higher photocurrents, with j_{sc} increasing from 10.0 (45 nm BHJ) to 12.1 mA cm^{-2} (65 nm BHJ), as reflected in the EQE (see Figure 13). The EQE illustrates that the increase of photocurrent is mainly from 500–800 nm, which corresponds to the Q-band of the phthalocyanine. The small differences in the wavelength range from 400–500 nm, where the fullerene C_{60} absorbs, are mainly attributed to minor shifts in the optical field distribution.

We attribute the increased j_{sc} compared to the unheated devices to a change in morphology, leading to a partial demixing

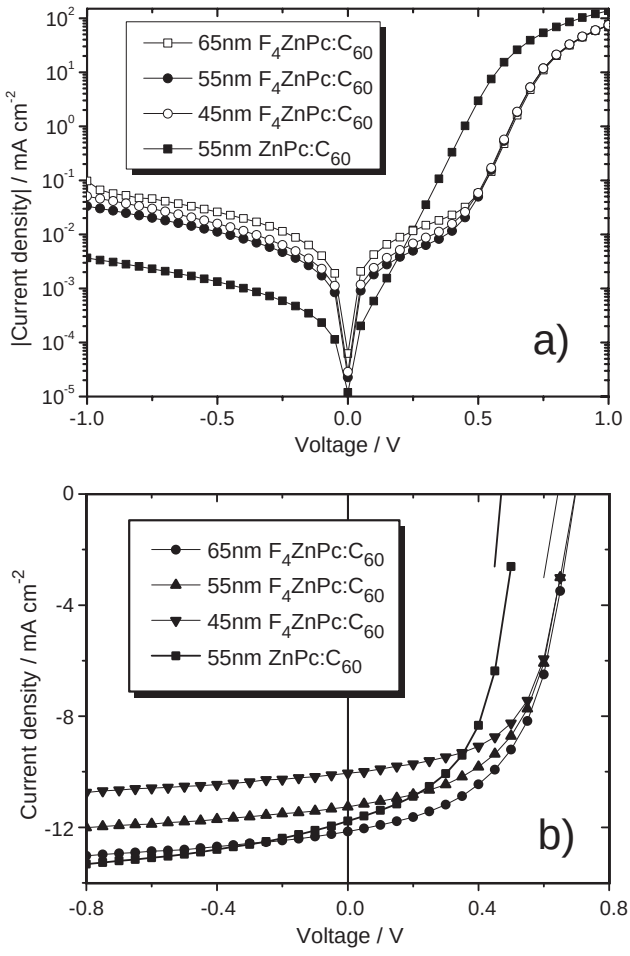

Figure 12. Current–voltage characteristics of a ZnPc:C_{60} based and several F_4ZnPc:C_{60} based devices in the dark (a) and under illumination (b) at t_{sub} = 104 °C.

of donor and acceptor and to a reduction of dead-ends. The interpenetrating network of donor and acceptor is hence well enough developed that even at high thicknesses, charge carriers can still be extracted. Compared to unheated devices, the OSC with t_b = 65 nm exhibits a 15% increased photocurrent (unheated: 10.6 mA cm^{-2}; heated: 12.1 mA cm^{-2}). For the same absorber thickness, j_{sc} is comparable to the reference ZnPc-based device, i.e., the OSC feature the same efficient exciton separation and charge carrier transport characteristics.

Table 2. Summary of the OSC parameters, averaged for 8 ZnPc:C_{60} and 15 F_4ZnPc:C_{60} devices. The thickness of the bulk heterojunction is given in brackets. All efficiencies are corrected for spectral mismatch. The F_4ZnPc devices were measured under 100 ± 1 mW cm^{-2}.

Device (t_b [nm])	V_{oc} [V]	j_{sc} [mA cm^{-2}]	*FF* [%]	η [%]
ZnPc (55)	0.52	11.8 ± 0.2	54	3.3 ± 0.1
F_4ZnPc (45)	0.68	10.0 ± 0.2	60	4.1 ± 0.1
F_4ZnPc (55)	0.68	11.3 ± 0.2	57	4.4 ± 0.1
F_4ZnPc (65)	0.69	12.1 ± 0.2	55	4.6 ± 0.1

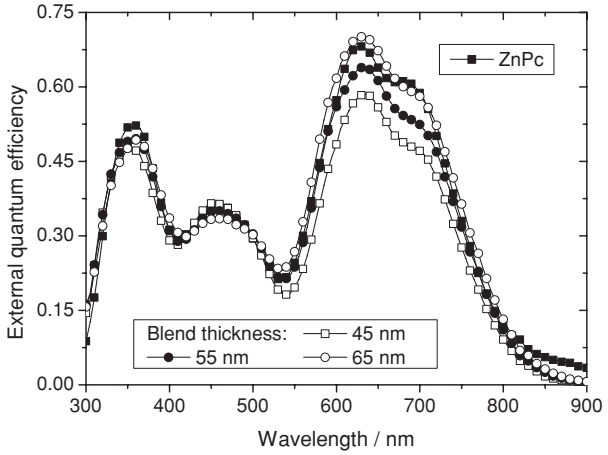

Figure 13. External quantum efficiency of heated F_4ZnPc:C_{60}-containing OSC. Blend thickness: Squares: 45 nm, circles: 55 nm, open circles: 65 nm.

All samples exhibit high FF > 54% even at t_b = 65 nm, resembling the results from an OSC with a 60 nm thick ZnPc:C_{60} blend, shown by Pfuetzner and co-workers, who obtained 57% FF with a heated substrate (110 °C) compared to 36% with an unheated device.[41] Fill factors above 55% are values that only the thinnest devices (t_b = 25 nm) achieve without substrate heating. In connection with the high current densities, this gives evidence that the blend layers consist of well-formed networks with good charge carrier percolation pathways. Substrate heating is known to support the layer formation in a positive way and favor a phase separation of the donor and acceptor constituents,[41] and we believe this to significantly contribute to the high efficiencies.

The j_{sc} and FF of F_4ZnPc-based OSC are comparable to ZnPc-based devices, with slightly lower photocurrents and higher FF if the donor is fluorinated. However, the strong increase of V_{oc} by around 30% leads to a 30% gain in efficiency from η = 3.3% (ZnPc) to η = 4.4% (F_4ZnPc) and opens a pathway for efficient single heterojunction OSC.

3. Conclusions

In summary, we show that fluorination of ZnPc to F_4ZnPc leads to a shift of the electron affinity and ionization potential, but does not substantially influence the optical gap. Hence, we can fabricate OSC with almost identical short circuit densities, but significantly higher open circuit voltages. OSC with F_4ZnPc:C_{60} BHJ exhibit power conversion efficiencies of 3.1–3.6% even without substrate heating, which is on par or superior to the best ZnPc-based devices found in the literature.

Furthermore, substrate heating during film deposition can be used to influence the BHJ morphology. This is reflected in the device performance: j_{sc} and FF are significantly increased, resulting in η = 4.6%. F_4ZnPc is a promising material and yields highly efficient single heterojunction OSC with excellent performance in the red spectral range, mainly owing to its positive susceptibility to heating and the very suitable energy levels.

4. Experimental Section

All devices are prepared in a multi-source vacuum chamber (K.J. Lesker, UK) on 15 × 15 cm^2 glass wafers that contain a prestructured ITO-coating (Thin Film Devices Ltd, USA). The wafers are cleaned in a multi-step wet process using acetone and ethanol, followed by an ozone treatment. The organic and metallic layers are deposited by vacuum sublimation (base pressure $\leq 10^{-7}$ mbar) through shadow masks. Depending on the ITO-pattern of the wafer, up to 6 × 6 different substrates (2.5 cm × 2.5 cm) can be prepared whereas each substrate consists of 4 identical solar cells. The solar cell area, defined by the overlap of ITO and metal contact, is 6.44 mm^2.

During deposition a flexible shutter system allows for different device stacks on the same wafer. One wafer is always processed completely without breaking the vacuum. Thus, comparable preparation conditions for all samples on one wafer are ensured. Layers for which specific temperatures are given are deposited at that substrate temperature. After the deposition process, wafers are transferred from the vacuum system directly to an attached glovebox with nitrogen atmosphere where the devices are encapsulated using UV-curing epoxy (Nagase) and a cover glass, including a moisture getter sheet (Dynic Ltd., China).

Three times sublimated ZnPc is purchased from Creaphys GmbH (Germany). F_4ZnPc is provided by BASF SE (Germany) and C_{60} bought from Bucky USA, all being purified three times by gradient vacuum sublimation (TGVS). Di-NPB is purchased from Sensient AG (Germany) and purified twice by TGVS.[19] The dopants NDP9 and NDN1 are purchased from Novaled AG (Germany) and used as received.

The samples for UV photoelectron spectroscopy (UPS) measurements are prepared in a multichamber UHV evaporation tool (Bestec, Germany) having a base pressure of 10^{-8} mbar. The UPS measurements are performed with a Phoibos 100 setup (Specs, Germany) at a base pressure of 10^{-10} mbar that is directly connected to the UHV evaporation tool. The setup is equipped with a helium discharge lamp with an excitation energy of 21.22 eV.

NDP9 and NDN1 are used because of better processability instead of the commonly used tetra-fluoro-tetracyano-quinodimethane (F_4-TCNQ) or WO_3 to p-dope materials with high IP and acridine orange base (AOB) as n-dopant for C_{60}. Their doping performance, however, is comparable.[49–51]

Calculations of device thin film optics are carried out using a simulation program based on the transfer matrix formalism. The optical constants of the organic materials are extracted from reflection and transmission measurements on pristine films with different known layer thicknesses and cross-checked with ellipsometry measurements. More details can be found elsewhere.[46,52,53] Optical constants of Al and ITO are taken from the commercially available ETFOS database, purchased from Fluxim AG (Switzerland). For the p-Di-NPB layers, *n* & *k* values with 5% p-doping are used, for n-C_{60} *n* & *k* values for pristine material is used. Due to the low doping concentration, the effect on the optical constants and the device optimisation due to differences in doping is minor.

Atomic force micrographs are recorded on a Nanoscope IIIa (Digital Instruments) in tapping mode. Scanning electron micrographs are recorded on a Zeiss GSM 982 Gemini. XRD measurements are performed in Bragg Brentano geometry using an XRD setup from Siemens (D5000) and Cu K_α radiation (40 kV/ 50 mA). All diffractograms are taken in steps of 0.4° from 3° to 40° (in 2θ) at a scanning speed of 5 s $step^{-1}$.

The IV measurements are carried out using a sun simulator (16S-150 V.3 by Solar Light Co., USA). The intensity is monitored by a Si diode that is calibrated using a certified reference diode from the Fraunhofer ISE CalLab, Germany.

To determine the external quantum efficiency and mismatch factor, a custom-made setup is used. The monochromatic beam (Oriel Xe Arc-Lamp Apex Illuminator combined with Cornerstone 260 1/4m monochromator, both Newport, USA) probing the device is chopped and the corresponding current response of the device measured via a lock-in amplifier 7265 DSP (Signal Recovery, UK). The EQE is measured without extra bias illumination.

Organic field effect transistor (OFET) chips from Fraunhofer IPMS (Dresden, Germany) with a bottom-gate and bottom-contact structure are used for mobility measurements, as described elsewhere.[41,54] The chips consist of a highly conductive p-doped Si wafer with a 230 nm thick thermally grown oxide. The oxide exhibits a capacity of 14.63 nF cm^{-2}. Au microstructures with a thickness of 30 nm for source and drain contact are prepared in a finger structure on top of the silicon dioxide. Due to this structure the channel width is 10 mm, while the channel length is varied between 5 and 20 µm. The substrates are chemically cleaned in an ultrasonic bath, followed by plasma cleaning. The organic materials are deposited on the chips in a UHV evaporation system. Finished samples are transferred to a measurement station under nitrogen atmosphere without exposure to air. The characteristics of the transistors are measured with two Keithley source measurement units.

Acknowledgements

This work received funding from the German Federal Ministry of Education and Research (BMBF) through the OPEG project (13N9716). We thank Ellen Kern from TU Dresden for SEM measurements; Jens Jankowski from TU Dresden for mobility measurements; Thomas Köhler and Christiane Müller from Bosch for XRD measurements; Selina Olthof from TU Dresden for assistance with UPS measurements; and Sudhakar Sundarray, Jaehyung Hwang and Peter Erk from BASF for providing F_4ZnPc.

Received: August 3, 2011
Revised: September 7, 2011
Published online: November 16, 2011

[1] C. W. Tang, *Appl. Phys. Lett.* **1986**, *48*, 183.
[2] D. Wynands, M. Levichkova, K. Leo, C. Uhrich, G. Schwartz, D. Hildebrandt, M. Pfeiffer, M. Riede, *Appl. Phys. Lett.* **2010**, *97*, 073503.
[3] R. Fitzner, E. Reinold, A. Mishra, E. Mena-Osteritz, H. Ziehlke, C. Koerner, K. Leo, M. Riede, M. Weil, O. Tsaryova, A. Weiss, C. Uhrich, M. Pfeiffer, P. Baeuerle, *Adv. Funct. Mater.* **2011**, *21*, 897.
[4] D. Cheyns, B. P. Rand, P. Heremans, *Appl. Phys. Lett.* **2010**, *97*, 033301.
[5] M. Riede, C. Uhrich, J. Widmer, R. Timmreck, D. Wynands, G. Schwartz, W.-M. Gnehr, D. Hildebrandt, A. Weiss, J. Hwang, S. Sudharka, P. Erk, M. Pfeiffer, K. Leo, *Adv. Funct. Mater.* **2011**, *21*, 3019.
[6] J. Meiss, T. Menke, K. Leo, C. Uhrich, W.-M. Gnehr, S. Sonntag, M. Pfeiffer, M. Riede, *Appl. Phys. Lett.* **2011**, *99*, 043301.
[7] M. A. Green, K. Emery, Y. Hishikawa, W. Warta, *Prog. Photovolt: Res. Appl.* **2011**, *19*, 84.
[8] P. Peumans, A. Yakimov, S. R. Forrest, *J. Appl. Phys.* **2003**, *93*, 3693.
[9] H. Brinkmann, C. Kelting, S. Makarov, O. Tsaryova, G. Schnurpfeil, D. Woehrle, D. Schlettwein, *Phys. Status Solidi A* **2008**, *205*, 409.
[10] A. Opitz, B. Ecker, J. Wagner, A. Hinderhofer, F. Schreiber, J. Manara, J. Pflaum, W. Bruetting, *Org. Electron.* **2009**, *10*, 1259.
[11] B. Yu, F. Zhu, H. Wang, G. Li, D. Yan, *J. Appl. Phys.* **2008**, *104*, 114503.
[12] I. Bruder, A. Ojala, C. Lennartz, S. Sundarraj, J. Schöneboom, R. Sens, J. Hwang, P. Erk, J. Weis, *Sol. Energy Mater. Sol. Cells* **2010**, *94*, 130.
[13] A. J. Ikushima, T. Kanno, S. Yoshida, A. Maeda, *Thin Solid Films* **1996**, *273*, 35.
[14] W. Gao, A. Kahn, *Appl. Phys. Lett.* **2001**, *79*, 4040.
[15] R. W. Lof, M. A. Van Veenendaal, B. Koopmans, H. T. Jonkman, G. A. Sawatzky, *Phys. Rev. Lett.* **1992**, *68*, 3924.
[16] J. X. Tang, Y. C. Zhou, Z. T. Liu, C. S. Lee, S. T. Lee, *Appl. Phys. Lett.* **2008**, *93*, 043512.
[17] J. Meiss, N. Allinger, C. Falkenberg, K. Leo, M. Riede, *Proc. SPIE* **2009**, *7416*, 741603–1.
[18] T. Taima, J. Sakai, T. Yamanari, K. Saito, *Sol. Energy Mater. Sol. Cells* **2009**, *93*, 742.
[19] J. Drechsel, A. Petrich, M. Koch, S. Pfützner, R. Meerheim, S. Scholz, K. Walzer, M. Pfeiffer, K. Leo, *SID Symp. Digest Tech. Pap.* **2006**, *37*, 1692.
[20] M. Egginger, R. Koeppe, F. Meghdadi, P. A. Troshin, R. N. Lyubovskaya, D. Meissner, N. S. Sariciftci, *Proc. SPIE* **2006**, *6192*, 61921Y-1.
[21] G. Dennler, H.-J. Prall, R. Koeppe, M. Egginger, R. Autengruber, N. Serdar Sariciftci, *Appl. Phys. Lett.* **2006**, *89*, 073502.
[22] B. Yu, L. Huang, H. Wang, D. Yan, *Adv. Mater.* **2010**, *22*, 1017.
[23] R. Schueppel, K. Schmidt, C. Uhrich, K. Schulze, D. Wynands, J. L. Bredas, E. Brier, E. Reinold, H.-B. Bu, P. Baeuerle, B. Maennig, M. Pfeiffer, K. Leo, *Phys. Rev. B* **2008**, *77*, 085311.
[24] K. Vandewal, K. Tvingstedt, A. Gadisa, O. Inganas, J. V. Manca, *Nat. Mater.* **2009**, *8*, 904.
[25] H. Ohkita, S. Cook, Y. Astuti, W. Duffy, S. Tierney, W. Zhang, M. Heeney, L. McCulloch, J. Nelson, D.D. C. Bradley, J. R. Durrant, *J. Am. Chem. Soc.* **2008**, *130*, 3030.
[26] T. Mayer, U. Weiler, C. Kelting, D. Schlettwein, S. Makarov, D. Wöhrle, O. Abdallah, M. Kunst, W. Jaegermann, *Sol. Energy Mater. Sol. Cells* **2007**, *91*, 1873.
[27] M. Pfeiffer, A. Beyer, T. Fritz, K. Leo, *Appl. Phys. Lett.* **1998**, *73*, 3202.
[28] R. Meerheim, S. Olthof, M. Hermenau, S. Scholz, A. Petrich, N. Tessler, O. Solomeshch, B. Luessem, M. Riede, K. Leo, *J. Appl. Phys.* **2011**, *109*, 103102.
[29] Q. L. Song, H. B. Yang, Y. Gan, C. Gong, C. M. Li, *J. Am. Chem. Soc.* **2010**, *132*, 4554.
[30] M. Koenemann, S. Sundarraj, J. H. Hwang, J. Schoeneboom, A. Liu, P. Peumans, F. Eickemeyer, I. Bruder, N. G. Pschirer, R. Sens, G. Weber, S. Bahulayan, P. Erk, *United States Patent US 2010/0207114A1* **2010**; http://www.freepatentsonline.com/y2010/0207114.html.
[31] D. Schlettwein, K. Hesse, N. E. Gruhn, P. A. Lee, K. W. Nebesny, N. R. Armstrong, *J. Phys. Chem. B* **2001**, *105*, 4791.
[32] Hyperchem program, release 4.5; PM3, next lowest state in the RHF approximation, gradient 10-3.
[33] W. Zhao, A. Kahn, *J. Appl. Phys.* **2009**, *105*, 123711.
[34] D. Veldman, S. C. J. Meskers, R. A. J. Janssen, *Adv. Funct. Mater.* **2009**, *19*, 1939.
[35] K. Vandewal, K. Tvingstedt, A. Gadisa, O. Inganäs, J. V. Manca, *Phys. Rev. B* **2010**, *81*, 125204.
[36] M. Hoffmann, K. Schmidt, T. Fritz, T. Hasche, V. M. Agranovich, K. Leo, *Chem, Phys. Lett.* **2000**, *258*, 73.
[37] K. Walzer, B. Maennig, M. Pfeiffer, K. Leo, *Chem. Rev.* **2007**, *107*, 1233.
[38] M. Riede, T. Mueller, W. Tress, R. Schueppel, K. Leo, *Nanotechnology* **2008**, *19*, 424001.
[39] K. Suemori, T. Miyata, M. Hiramoto, M. Yokoyama, *Jpn. J. Appl. Phys.* **2004**, *43*, L1014.
[40] S. Pfuetzner, J. Meiss, A. Petrich, M. Riede, K. Leo, *Appl. Phys. Lett.* **2009**, *94*, 253303.
[41] S. Pfuetzner, C. Mickel, J. Jankowski, M. Hein, J. Meiss, C. Schuenemann, C. Elschner, A. A. Levin, B. Rellinghaus, K. Leo, M. Riede, *Org. Electron.* **2011**, *12*, 435.
[42] C. Schuenemann, C. Elschner, A. A. Levin, M. Levichkova, K. Leo, M. Riede, *Thin Solid Films* **2011**, *519*, 3939.
[43] I. Bruder, J. Schöneboom, R. Dinnebier, A. Ojala, S. Schäfer, R. Sens, P. Erk, J. Weis, *Org. Electron.* **2010**, *11*, 377.
[44] P. Erk, Private communication, to Cambridge Crystallographic Data Center (CCDC; reference code: CUPOCY14).

[45] D. Raoufi, A. Kiasatpour, H.R. Fallah, A. S. H. Rozatian, *Appl. Surf. Sci.* **2007**, *253*, 9085.
[46] B. Maennig, J. Drechsel, D. Gebeyehu, P. Simon, F. Kozlowski, A. Werner, F. Li, S. Grundmann, S. Sonntag, M. Koch, K. Leo, M. Pfeiffer, Ha. Hoppe, D. Meissner, N. S. Sariciftci, I. Riedel, V. Dyakonov, J. Parisi, *Appl. Phys. A* **2004**, *79*, 14.
[47] P. Simon, B. Maennig, H. Lichte, *Adv. Funct. Mater.* **2004**, *14*, 669.
[48] S. Schäfer, A. Petersen, T. A. Wagner, R. Kniprath, D. Lingenfelser, A. Zen, T. Kirchartz, B. Zimmermann, U. Würfel, X. Feng, T. Mayer, *Phys. Rev. B* **2011**, *83*, 165311.
[49] G. Schwartz, T. H. Ke, C. C. Wu, K. Walzer, K. Leo, *Appl. Phys. Lett.* **2008**, *93*, 073304.
[50] S. Reineke, F. Lindner, G. Schwartz, N. Seidler, K. Walzer, B. Lüssem, K. Leo, *Nature* **2009**, *459*, 234.
[51] J. Meyer, S. Hamwi, S. Schmale, T. Winkler, H.-H. Johannes, T. Riedl, W. Kowalsky, *J. Mater. Chem.* **2009**, *19*, 702.
[52] T. Fritz, J. Hahn, H. Böttcher, *Thin Solid Films* **1989**, *170*, 249.
[53] R. Schueppel, R. Timmreck, N. Allinger, T. Mueller, M. Furno, C. Uhrich, K. Leo, M. Riede, *J. Appl. Phys.* **2010**, *107*, 044503.
[54] M. S. Wrackmeyer, M. Hein, A. Petrich, J. Meiss, M. Hummert, M. K. Riede, K. Leo, *Sol. Energy Mater. Sol. Cells* **2011**, *95*, 3171.